Raman scattering in β-ZnS

J. Serrano,[1] A. Cantarero,[2] M. Cardona,[1] N. Garro,[2] R. Lauck,[1] R. E. Tallman,[3] T. M. Ritter,[4] and B. A. Weinstein[3]
[1]*Max Planck Institut für Festkörperforschung, Heisenbergstrasse 1, 70569 Stuttgart, Germany*
[2]*Institut de Ciència dels Materials, Universitat de València, P.O. Box 22085, E-46071 Valencia, Spain*
[3]*Department of Physics, SUNY at Buffalo, Buffalo, New York 14260, USA*
[4]*Department of Chemistry and Physics, UNC Pembroke, North Carolina 28372, USA*
(Received 1 October 2003; published 22 January 2004)

The first- and second-order Raman spectra of cubic ZnS (β-ZnS, zinc-blende) are revisited. We consider spectra measured with two laser lines for samples with different isotopic compositions, aiming at a definitive assignment of the observed Raman features and the mechanisms which determine the linewidth of the first order TO and LO Raman phonons. For this purpose, the dependence of the observed spectra on temperature and pressure is investigated. The linewidth of the TO phonons is found to vary strongly with pressure and isotopic masses. Pressure runs, up to 15 GPa, were performed at 16 K and 300 K. Whereas well-defined TO Raman phonons were observed at low temperature in the whole pressure range, at 300 K the TO phonons appear to hybridize strongly with the two-phonon background and lose their identity, especially in the (3–10)-GPa region. The intensity of the TO phonons, which nearly vanishes when measured with a red laser line, is shown to result from a destructive interference of the amplitudes of the band-edge resonance and that of a background of opposite sign. The analysis of these effects is aided by calculations of the densities of one- and two-phonon states performed with the adiabatic bond charge model of the lattice dynamics.

DOI: 10.1103/PhysRevB.69.014301 PACS number(s): 78.30.Fs, 63.20.Ry, 63.20.Kr

I. INTRODUCTION

Zinc sulfide is found in nature as zinc-blende (also called sphalerite, β-ZnS, with cubic structure) and as wurtzite (2H, hexagonal, α-ZnS). The names of these minerals are used to designate the corresponding crystal structures. ZnS, both natural and synthetic, crystallizes in as many as ten different polytypes[1–3] and mixed crystals, transforming from one structure to another at stacking faults.[3]

Large good quality β-ZnS crystals are found in nature and can also be grown in the laboratory at relatively low temperature.[4] Investigations of their lattice vibrations were started early and are of interest because this material is the prototype of the important zinc-blende family of semiconductors. Such investigations were performed by ir (Ref. 5) and Raman[6–9] spectroscopies. In Ref. 8 Raman measurements of β-ZnS were combined with measurements of the 4H and 6H polytypes to obtain information about the phonon-dispersion relations of β-ZnS along the [111] direction of its Brillouin zone (BZ). Raman measurements for the wurtzite modification were published by Poulet *et al.*[10] and by Arguello *et al.*[11] These measurements provide the phonon frequencies only at a few points of the BZ. Information across the whole Brillouin zone has been obtained by inelastic neutron scattering (INS) using large (but rather imperfect) natural and synthetic single crystals.[12,13] These INS data have been fitted with phonon-dispersion relations based on shell models.[13] More recently, the INS data of Ref. 13 have been fitted with a six-parameter bond charge model (BCM) and the corresponding dispersion relations have been used to calculate the one-phonon density of states for β-ZnS and other zinc-blende-type crystals.[14]

In this work we present Raman spectra of β-ZnS prepared with different isotopic compositions (nominal compositions $^{nat}Zn^{nat}S$, $^{68}Zn^{nat}S$, $^{64}Z^{34}S$, $^{68}Zn^{34}S^{nat}_{0.5}S_{0.5}$). We give in Table I the average isotopic masses of these four samples and the corresponding mass fluctuation parameters $g^{(2)}_{Zn}$ and $g^{(2)}_{S}$.[15] Measurements were performed with two different laser lines (red, 647.1 nm, and green, 514.5 nm), at several temperatures in the (6–300)-K range and under hydrostatic pressures from 0 to 15 GPa (see also Refs. 16 and 17). They encompass the TO and LO Raman phonons as well as spectra corresponding to sums (overtones and combinations) and differences of two phonons.[16,18] We also report calculations, based on the BCM lattice dynamics, of the densities of states (DOS's) for sums and differences of two phonons with total **q** equal to zero. The calculations were performed for the various isotopic compositions under consideration. They have been used for the interpretation of the second-order Raman spectra and also of the linewidths of the TO(Γ) and LO(Γ) phonons vs pressure, temperature, and isotopic mass. The following results have been obtained.

(1) The vanishing of the TO(Γ) intensity for laser frequencies in the red ($\sim$1.95 eV) has been confirmed.[7,16] It can be attributed to a destructive interference of a nonresonant-scattering amplitude with the term that resonates at the band gap. The introduction of this nonresonant amplitude changes the value of the electron-phonon deformation potential $d_0=4$ eV reported in Ref. 19 to d_0

TABLE I. Compositions and mass fluctuation parameters $g^{(2)}$ of our ZnS samples. The masses and isotope abundances were obtained from Ref. 43. Natural S contains 95% of ^{32}S, 0.8% of ^{33}S, and 4.2% of ^{34}S. Throughout this work we have used ^{34}S and ^{nat}S. Because of its similarity to ^{32}S we shall label ^{nat}S as ^{32}S.

Nominal compositions	$\langle M_{Zn}\rangle$	$\langle M_S\rangle$	$g^{(2)}_{Zn}$	$g^{(2)}_{S}$
$^{nat}Zn^{nat}S$	65.41	32.07	6.0×10^{-4}	1.7×10^{-4}
$^{68}Zn^{nat}S$	67.92	32.07	0	1.7×10^{-4}
$^{64}Z^{34}S$	63.93	33.97	0	0
$^{68}Zn^{34}S^{nat}_{0.5}S_{0.5}$	65.41	33.02	0	9.1×10^{-4}

$\simeq$16 eV, more in line with calculated values and with the systematics of d_0 for the zinc-blende-type materials.

(2) The widths of the LO(Γ) Raman phonons are shown to be determined by two decay channels: (a) decay into 2LA-phonon overtones and (b) decay into TA+TO combinations. At 16 K these linewidths increase with increasing pressure, reaching a maximum at about 3.5 GPa. They decrease above this pressure, reaching a minimum at 5.5 GPa, a maximum at 8.5 GPa, and another broad minimum at 10 GPa. This effect can be qualitatively explained on the basis of the calculated densities of two-phonon states and the measured pressure dependence of the LO(Γ) frequencies and those of the 2LA and TA+TO critical points.[16,17] The calculated two-phonon DOS's also explain the dependence of the widths on isotopic masses for the two isotopically pure crystals measured, as well as the natural crystal.

(3) The Raman spectrum of the TO(Γ) phonon shows a larger width than the LO(Γ) spectrum at atmospheric pressure, even at low temperature. This reflects strong decay processes for the TO phonons into two-phonon states, which have been identified as TA+LA combinations. This phenomenon is similar to that observed for GaP.[16,20] The width of the TO peak varies slightly with isotopic composition and, most strikingly, it increases upon the application of pressure. At 16 K, nearly Lorentzian TO peaks can be observed throughout the whole pressure range, with full width at half maximum-(FWHM) between 1.5 and 7.5 cm^{-1}, displaying maxima at 4 and 9 GPa. At 300 K the TO peak mixes for a pressure $p \simeq 3.5$ GPa with the two-phonon background, made strongly Raman active by the admixture with TO(Γ) phonons. The bare frequency of the TO(Γ) phonon increases with pressure faster than that of the TA+LA background, a fact which leads to the reappearance of a sharpened TO(Γ) peak above the two-phonon band at $p > 10$ GPa. These observations have been quantitatively interpreted on the basis of a Fermi resonance involving the calculated two-phonon DOS. The anharmonic coupling constant $|V_3|^2 = 90\ cm^{-2}$ is in line with that found for GaP, CuCl, and CuBr.[20–22]

(4) Several features of the two-phonon Raman spectra have been interpreted on the basis of their dependence on pressure, temperature, and isotopic mass. In particular, we have confirmed the assignment[17] of the peak observed for natural ZnS at 220 cm^{-1} under normal conditions to differences of TO and TA phonons: the peak disappears at $T = 0$ K and shifts with pressure at a rate higher than that of the zone-edge TO phonons. Its dependence on isotopic mass also signals the correspondence to scattering by TO-TA difference modes. Other second-order structures observed in the Raman spectra have been reliably assigned on the basis of the calculated two-phonon densities of states. Special attention has been paid to the high-frequency end of the two-phonon spectrum, which consists of scattering by two LO(Γ) phonons, and its dependence on isotopic mass.

(5) Whereas no effects of the isotopic disorder on the linewidths of the TO(Γ) and LO(Γ) peaks have been identified, even for the $^{68}Zn^{32}S^{34}_{0.5}S_{0.5}$ sample, effects on their frequencies have been observed for this sample. They have been assigned to the real part of the self-energy associated with the isotopic disorder.

II. EXPERIMENTAL DETAILS

A. Sample preparation

In order to grow cubic ZnS crystals, the temperature must be kept below 800 °C.[23] Therefore, sublimation is not possible and chemical vapor transport must be applied as a growth method for bulk material.[24–27]

Several processes are performed preceding growth: Elemental sulfur is purified by sublimation at 90–150°C. The 1:1 mixture of ^{32}S and ^{34}S is produced by multiple sublimation, followed by melting and rolling in a fused silica ampoule. Small pieces of Zn metal ($\leqslant 0.2$ g) are etched in propanol with 1–5 % nitric acid, under ultrasonic shaking to remove possible oxide layers. A further purification is achieved by sublimation in a fused silica ampoule, followed by separation of the residue.

The resulting porous layer of Zn favors the synthesis reaction under sulfur vapor pressures of 3–450 mbar. For this purpose, the zinc end of the ampoule is heated stepwise up to about 1000 °C. The formation of a ZnS passivation layer prevents the evaporation of the metal and controls the progressing reaction by solid-state diffusion of the Zn atoms through this layer. The synthesis must be complete because it is found that a metal excess of a few milligrams drastically decreases the growth rate.

At a maximum temperature of 400 °C, the stoichiometry is adjusted by vacuum annealing. The portion of the synthesis ampoule with ZnS is placed into a growth ampoule with an inner diameter of 10–12 mm and a length of about 350 mm. By using iodine (0.3–2 mg/cm^3) as a transporting agent, the growth of transparent colorless, yellowish, and greenish crystals, up to 5 mm in length and with (100), (110), and (111) facets, takes place in the temperature range of 650–750 °C, at a source temperature of 750–850 °C. The presence of 350–700 mbar of argon and a low-temperature gradient limit the transport rate (maximum 3.3 $mg/h\,cm^2$), and also the number of nucleation centers, as desired. The samples used in this work are listed in Table I.

B. Experimental details

The Raman spectra of a sample with natural isotopic composition were measured with an XY-Dilor triple spectrometer equipped with a nitrogen cooled charged-coupled device-(CCD). The sample was kept in a microscope cryostat and its temperature varied from 4 to 300 K. The incoming polarization was rotated by means of a $\lambda/4$ plate in order to measure both $x(z,z)\bar{x}$ and $x(y,z)\bar{x}$ scattering configurations. The 514.5-nm line of an Ar^+-ion laser was used as excitation source. The samples with variable isotopic compositions were measured with a SPEX Triplemate spectrometer, also equipped with a nitrogen cooled CCD. These samples were measured in a microscope cryostat at temperatures from 80 to 300 K. The temperature control was better than ± 0.2 K. In this case the different lines of a mixed Ar^+-Kr^+-ion laser were used.

The high-pressure measurements were performed in diamond anvil cells using helium and a 4:1 methanol-ethanol mixture as pressure transmitting medium at low and room

temperature, respectively. The excitation source was the 514.5-nm line of an Ar^+-ion laser, and a double-grating spectrometer (ISA JOBIN YVON U1000) was used to analyze the scattered light, which was collected by a Princeton Instruments multichannel detector consisting of a Peltier-cooled photocathode and a microchannel plate intensifier with a Si diode array readout. The typical sample sizes used in the measurements were $60\times60\times30$ μm^3. The samples were loaded under a microscope in inconel gaskets together with a small ruby crystal utilized as reference for the determination of pressure.[28] The pressure was applied by a hydraulic pump operated with oil, which transferred the force to a steel tube pushing the upper diamond against the gasket and lower diamond.[29]

The analysis of the Raman spectra was performed after calibration with the emission lines of a low-density neon gas lamp. These lines were fitted to a Gaussian profile, the resulting width being the spectral resolution, which will be indicated in the description of the experimental data. The Raman peaks were fitted to Voigt profiles, i.e., a convolution of a Lorentzian with a Gaussian, the latter having as width the spectral resolution.

III. DENSITY OF TWO-PHONON STATES

The density of two-phonon states subject to the constraints $\omega=\omega_1\pm\omega_2$ (plus sign for sum processes and minus sign for difference processes) and $\mathbf{q}_1=\pm\mathbf{q}_2$ was calculated using the bond charge model parameters of the dispersion relations given by Rajput and Browne.[14] For the **q**-space integration we used the tetrahedron method with 3345 points in the irreducible Brillouin zone. The DOS calculated for natural ZnS are shown in Fig. 1(a) for difference processes and Fig. 1(b) for sum processes.

We have also calculated, employing the same force constants, the two-phonon DOS for the two isotopically pure samples used in our experiments, namely, $^{68}Zn^{32}S$ and $^{64}Zn^{34}S$. Instead of presenting them here as figures similar to Fig. 1 , we find it more useful to give in Table II the positions of the most prominent peaks and thresholds and their assignments on the basis of the dispersion relations.[30]

We discuss next some interesting features of the isotope effects on the two-phonon frequencies listed in Table II. First, we note that the isotope shifts of the $2LO_\Gamma$ (7 ± 1 cm^{-1}) and the $2TO_\Gamma$ (6 ± 1 cm^{-1}) agree reasonably well with those calculated from the corresponding reduced masses (5.9 cm^{-1} for $2LO_\Gamma$ and 4.7 cm^{-1} for $2TO_\Gamma$). The structure found at 702 cm^{-1} for natural ZnS, only 10 cm^{-1} below that for the $2LO_\Gamma$, has been assigned to $2LO_L$. For the latter overtone mode, it is interesting to note that the shift of 20 cm^{-1} between $^{68}Zn^{32}S$ and $^{64}Zn^{34}S$, much larger than that calculated for $2LO_\Gamma$, reflects only the effect of the change in the sulfur mass (19 cm^{-1}); we can thus conclude that the eigenvector of the LO_L phonon does not significantly involve the motion of the Zn atoms. The same thing can be said for the LO_X and LO_Σ phonons. Although, by symmetry, these eigenstates mix with the corresponding LA states (mainly Zn-like, see below) the admixture is negligible because of the large difference between the Zn and S masses.

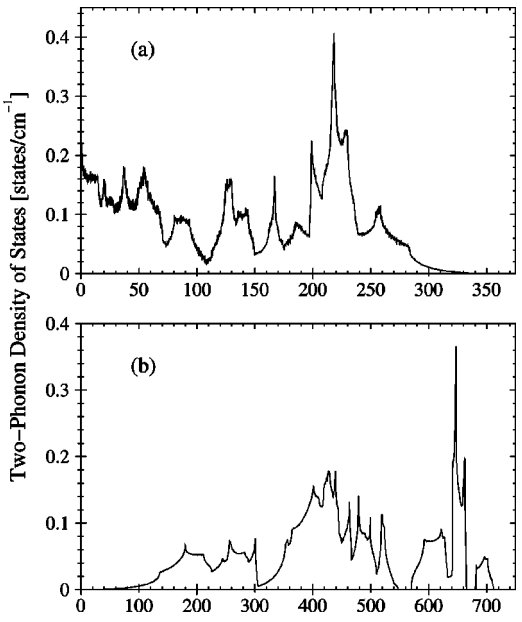

FIG. 1. (a)Two-phonon difference (with $\mathbf{q}_1-\mathbf{q}_2=0$) and (b) sum (with $\mathbf{q}_1+\mathbf{q}_2=0$) densities of states of natural ZnS obtained from the semiempirical dispersion relations in Ref. 14. No corrections for differences between the calculations in Ref. 17 and the INS data on which they are based have been performed. These differences amount to as much as 20 cm^{-1} for some of the critical points. The most important features, some of which have been observed in the experiment, are summarized in Table II.

The corresponding shifts read off Table II for the $2TO_X$ and $2TO_L$ peaks are 14 and 11 cm^{-1}, respectively; the predictions based on the sulfur mass are larger (17 and 16 cm^{-1}, respectively). This indicates a larger admixture of Zn motion to these modes than for the corresponding LO modes. For the 2TA peaks we find shifts of -4 cm^{-1} both at *X* and at *L*. The shifts calculated from the Zn masses are -5.5 cm^{-1} and -4.3 cm^{-1}, respectively. The differences between the two sets of shifts reflect the admixture of a small amount of sulfur motion in the corresponding eigenvectors.

We also note that the isotope shift reverses sign at a frequency between $[LA+TA_u]_\Sigma$ (301 cm^{-1}) and $[TO+TA]_X$ (401 cm^{-1}), corresponding to the fact that the eigenvectors of the acoustic phonons are Zn-like while those of the optic ones are S-like.

In Fig. 2(a) we display the calculated two-phonon sum DOS for three of the samples under consideration in the (275–400)-cm^{-1} region which encompasses the frequencies of the TO_Γ and LO_Γ phonons and the shift reversal region. The curves in Fig. 2(a) shift monotonically with each of the isotopic masses, except for the structures in the (340–370)-cm^{-1} region which fall in the range where the isotope shifts change sign. These structures change monotonically between $^{68}Zn^{32}S$ and the natural sample; they consist in these cases of a plateau and a square-root threshold (at 356 and 368 cm^{-1}, respectively, for the natural sample). The plateau is assigned to $2LA_W$ modes and the threshold to $[TO+TA]_L$. The former are Zn-like and thus shift up from $^{68}Zn^{32}S$ to $^{64}Zn^{34}S$, whereas the latter are partly sulfur-like (TO) and Zn-like (TA). Hence, there is a partial compensa-

TABLE II. Phonon combinations corresponding to different critical points which produce a peak (Van Hove singularity) in the density of two-phonon states obtained for several isotopic compositions, using the BCM parameters of Ref. 14. The subindices "*u*" and "*l*" indicate the upper and lower transverse branches, respectively.

Overtones and combinations	Energy position (in cm^{-1})			Overtones and combinations	Energy position (in cm^{-1})			Phonon difference	Energy position (in cm^{-1})		
	$^{64}Zn^{34}S$	$^{nat}Zn^{nat}S$	$^{68}Zn^{nat}S$		$^{64}Zn^{34}S$	$^{nat}Zn^{nat}S$	$^{68}Zn^{nat}S$		$^{64}Zn^{34}S$	$^{nat}Zn^{nat}S$	$^{68}Zn^{nat}S$
$2LO_\Gamma$	702	712	709	$[LO+TA]_L$	456	464	462	$[LO-TA]_L$	272	281	282
$2LO_L$	682	702	702	$[LO+TA]_X$	429	439	440	$[LO-TA]_X$	248	257	259
$2LO_X$	678	697	698	$[TO+TA]_X$	394	401	401	$[TO-TA]_X$	210	218	220
$2LO_\Sigma$	664	682	682	$[TO+TA]_L$	359	368	366	$[TO-TA_u]_\Sigma$	188	199	198
$LO+TO_X$	645	662	662	$2LA_W$	359	356	349	$[LO-LA]_\Sigma$	155	167	162
$[LO+TO]_L$	630	647	647	$[LA+TA_u]_{W,\Sigma}$	304	301	295	$[TO_u-LA]_\Sigma$	133	143	147
$2TO_X$	608	622	622	$[LA+TA_l]_W$	282	281	276	$[TO_l-LA]_\Sigma$	118	127	129
$2TO_L$	580	593	591	$[LA+TA_l]_\Sigma$	258	256	251	$[LA-TA_l]_\Sigma$	92	93	94
$2TO_\Gamma$	561	570	567	$[2TA_u]_\Sigma$	246	244	239	$[LO-TO]_L$	52	55	55
$[LO+LA]_\Sigma$	513	519	516	$[2TA_l]_W$	212	211	207	$[LO-TO]_X$	34	37	39
$[TO_u+LA]_\Sigma$	492	499	496	$2TA_X$	181	180	177	$[LO-TO_u]_\Sigma$	21	20	21
$[TO_l+LA]_\Sigma$	475	479	476	$2TA_L$	138	137	134	$[TO_u-TO_l]_\Sigma$	13	14	16

tion in the shift of this mode with predominance of the sulfurlike shift because the TO_L frequency is higher than the TA_L frequency. Accidentally, the two features coincide for the $^{64}Zn^{34}S$ sample, giving a strong peak at 359 cm^{-1}. This fortuitous coincidence would be lifted by the application of pressure.[17,16]

The DOS of the difference modes is shown in Fig. 1(a) for the natural sample. It is dominated by a strong peak at 218 cm^{-1} which will be the strongest structure in the two-phonon difference Raman spectra (see Sec. VII). The shift of this feature from $^{64}Zn^{34}S$ to $^{68}Zn^{32}S$, 10 cm^{-1}, and also the shift of most peaks in this difference DOS, is much larger than that of the peaks in the sum DOS at similar frequencies (-3 cm^{-1}) and has the opposite sign. This behavior will enable us in Sec. VII to identify the difference modes in the two-phonon Raman spectra.

When comparing the DOS of Figs. 1 and 2 and the frequencies of Table II with experimental data, one must keep in mind that the dispersion relations calculated in Ref. 14 for natural ZnS, using a rather small number of adjustable parameters (six), do not exactly fit the available INS data. We can read from Fig. 1 of Ref. 14 that the calculated LO_Γ and TO_Γ frequencies lie about ≈ 6 cm^{-1} above the experimental points (measured at 300 K). This explains the differences between the $2LO_\Gamma$ and $2TO_\Gamma$ frequencies of Table II and twice those listed in Table III. The largest differences are found for the LO_X and LA_X modes: the calculated LO_X mode lies 18 cm^{-1} higher than the measured point, whereas the corresponding LA_X mode lies 12 cm^{-1} lower. Similar differences are found at the L point: LO_L is 12 cm^{-1} higher whereas LA_L is 8 cm^{-1} lower. Appropriate corrections must be applied to the frequencies of Table II before comparing them with the two-phonon Raman-scattering data. We shall see that these corrections considerably improve the agree-

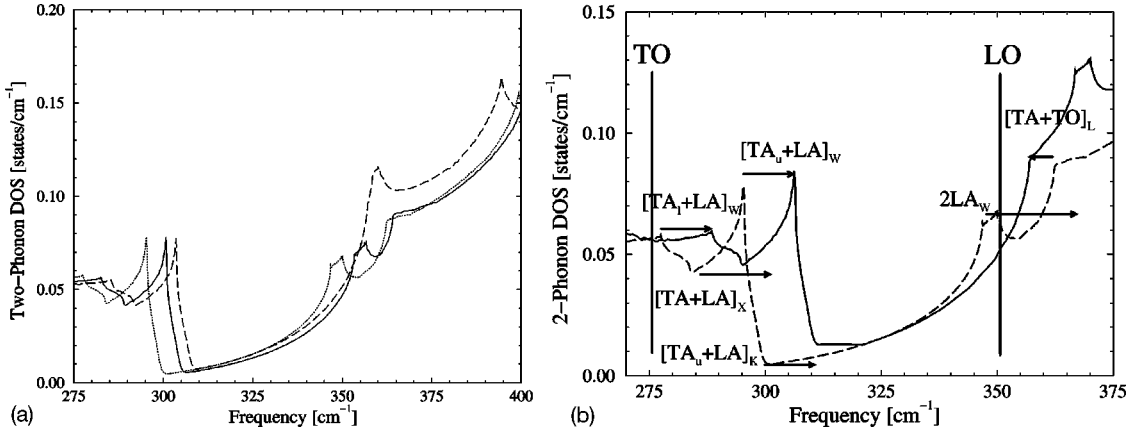

FIG. 2. (a) Two-phonon sum density of states corresponding to natural ZnS (solid), $^{68}Zn^{nat}S$ (dotted), and $^{64}Zn^{34}S$ (dashed). Only the region close to the TO and LO Raman peaks is shown to facilitate the later discussion of the effect of the DOS on the phonon broadening. (b) Two-phonon sum DOS of natural ZnS in the region of the TO_Γ and LO_Γ phonons (vertical lines), before (dashed curve) and after (solid curve) correcting the dispersion relations as indicated in the text. Note that the $2LA_W$ peak shifts to the other side of the $[TA+TO]_L$ threshold after the correction of the dispersion relations discussed in the text.

TABLE III. Frequencies and linewidths (FWHM, in parentheses) measured in cm^{-1} for the TO and LO Raman phonons of several isotopically modified samples of Table I. The error bars for the frequencies are $\pm 0.5\ cm^{-1}$. Those for the linewidths are $0.5\ cm^{-1}$ (TO) and $0.2\ cm^{-1}$ (LO).

		16 K	80 K	300 K
$^{64}Z^{34}S$	TO	273.1 (1.9) [a]	273.0 (2.6)	270 (9.3)
	LO	347.5 (0.7) [a]	347.4 (0.9)	345 (2.9)
$^{68}Zn^{nat}S$	TO	275.6 (3.7)	275.6 (4.0)	273 (12.2)
	LO	350.6 (0.7)	350.6 (1.1)	348 (3.3)
$^{68}Zn^{32}S_{0.5}^{34}S_{0.5}$	TO	272.5 (2.3) [a]	272.5 (3.1)	269.5 (11.6)
	LO	348 (0.8) [a]	348 (1.0)	345.6 (3.3)
$^{nat}Zn^{nat}S$	TO	277.5 (3.3)	277.4 (4.0)	275 (10.8)
	LO	353 (0.7)	353 (0.85)	350 (3.3)

[a]Data extrapolated from those at 80 K by using the appropriate Bose-Einstein factors.

ment between the frequencies of Table II and the experimental data.

The sum DOS of Fig. 2(a) will be used in Sec. VII to interpret the phonon linewidths and their dependence on pressure and isotopic composition. Before doing that, the corrections just mentioned must also be applied. Figure 2(b) displays the relevant portion of this DOS before and after applying such corrections for natural ZnS.

IV. TO AND LO RAMAN PHONONS

A. Experimental results

Typical first-order spectra measured at 80 K with the 514.5-nm laser line are shown for four isotopic compositions in Fig. 3. The resolution used for these measurements was $0.8 \pm 0.1\ cm^{-1}$ FWHM. Note that the integrated strengths of the TO peaks are one order of magnitude weaker than for the LO peaks (this will be discussed in Sec. IV B) and are superimposed on a weak background, which we attribute to the decay channel provided by the two-phonon density of states [see Fig. 2(b)]. The frequencies of the eight peaks in Fig. 3 and their widths, obtained after deconvolution using Voigt profiles, are listed in Table III.

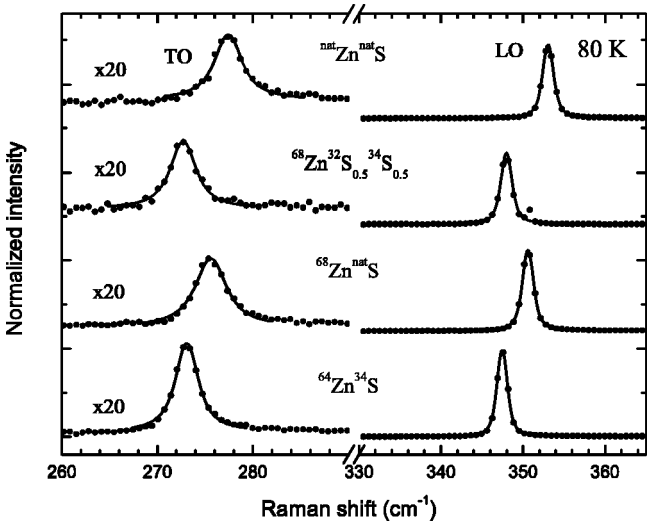

FIG. 3. Raman spectra of β-ZnS for several isotopic compositions at 80 K, as measured (see Table III for deconvoluted widths). The solid lines are fits with a Voigt function, using $0.8\ cm^{-1}$ for the spectral resolution.

Part of the initial motivation of this work was to investigate whether the LO and/or TO linewidths depend on isotopic mass: A strong dependence had been observed for the TO modes[20] of GaP and the E_2^{upper} modes[31] of wurtzite-type ZnO. According to Table III, a dependence of width on isotopic mass takes place for the TO phonon, but the spectral resolution is too low to allow any conclusions concerning the LO phonon.

B. Antiresonant behavior of the TO phonons

According to Fig. 3 the ratio of the TO and LO integrated intensities is $I_{TO}/I_{LO}=0.10$ at $\hbar\omega_L=2.41$ eV. We find from Fig. 1 of Ref. 19 at this laser frequency $I_{LO}=10^{-10}\omega_L^4\ cm^{-1}\ sr^{-1}$. This figure enables us to obtain experimental values for I_{LO} at several energies in the range $2.5 \leqslant \hbar\omega_L \leqslant 3.8$ eV. We have not detected any I_{TO} intensity for $\hbar\omega_L=1.96$ eV, in agreement with the result of Ref. 19. This behavior can be accounted for with the expressions [see Eq. (7) of Ref. 19]

$$I_{TO}(\omega)=d_0^2[-Ag_0(x)-B]^2,$$

$$g_0=x^{-2}[2-(1-x)^{-1/2}-(1+x)^{-1/2}], \quad x=\omega_L/\omega_0, \tag{1}$$

where d_0 is the corresponding electron-phonon deformation potential[32] and $\hbar\omega_0$ is the energy of the direct gap, $\hbar\omega_0=3.8$ eV at 300 K for β-ZnS. Note that Eq. (1) is a simplification of Eq. (7) of Ref. 19, obtained under the reasonable assumption of a negligible spin-orbit splitting. An expression for A, taken to be positive, can be found in Ref. 19. The first term in brackets in Eq. (1) is positive, since $Ag_0(x)$ is negative, and increases rapidly with increasing ω_L. Hence, a positive and sufficiently large value of B leads to an antiresonance and a zero intensity for a value of $\omega_L<\omega_0$. We adjust the value of B so as to bring this zero of intensity to $\hbar\omega_L \simeq 1.95$ eV, as required semiquantitatively by the absence of TO intensity at this frequency.

This treatment of the data of Ref. 19 leads to $|d_0|=18$ eV, instead of the value $|d_0|=4$ eV which disagreed with theoretical calculations.[19,32] The new value of d_0, obtained after taking into account the antiresonance, is compatible with the value of $d_0=+24$ eV calculated in Ref. 32.

V. PRESSURE DEPENDENCE OF THE TO- AND LO-PHONON FREQUENCIES AND LINEWIDTHS

A. Experimental results

Measurements at several pressures were performed at 300 K (up to 12 GPa) and at 16 K (up to 15 GPa). Figure 4 shows the low-temperature spectra obtained at several representative pressures. This figure reveals the nonmonotonic behav-

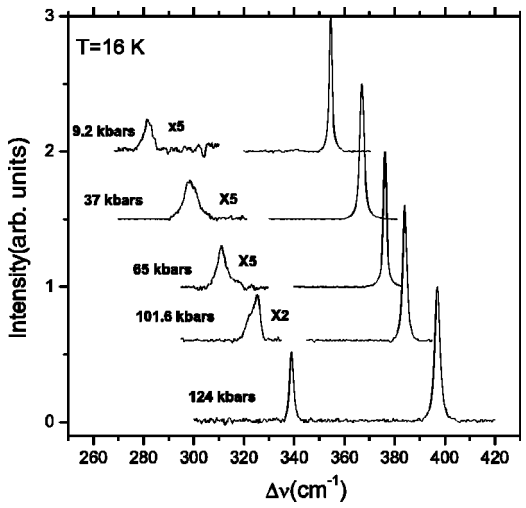

FIG. 4. Raman spectra of the LO and TO phonons of $\beta-{}^{68}Zn^{32}S$ measured for several pressures at 16 K with the 514.5-nm laser line. The spectra are unsmoothed: the instrument resolution of 1.1 cm^{-1} FWHM has not been deconvoluted.

ior of the linewidth vs pressure as displayed in Fig. 5. We have plotted in Fig. 6 the measured variation of the TO- and LO-phonon frequencies with pressure, which agrees with the measurements and calculations of Weinstein.[16] Like in most zinc-blende-type semiconductors, the LO-TO splitting decreases with increasing pressure, a fact which will be discussed below. By fitting the measured dependence of the phonon frequencies on pressure we obtain the following expressions for the frequencies vs p (GPa):

$$\omega_{\mathrm{LO}}\ (300\ \mathrm{K}) = 347.2(7) + 4.7(3)p - 0.05(2)p^2,$$

$$\omega_{\mathrm{LO}}\ (16\ \mathrm{K}) = 350.6(4) + 4.3(1)p - 0.04(1)p^2,$$

$$\omega_{\mathrm{TO}}\ (16\ \mathrm{K}) = 275.6(7) + 6.1(2)p - 0.08(1)p^2. \qquad (2)$$

Figure 7(a) displays spectra measured at 300 K for different pressures in the (0.3–11)-GPa range obtained with a resolution of 1.7 cm^{-1} (FWHM), which has not been deconvoluted. The linewidth of the LO peak is seen to vary rather smoothly with increasing pressure, whereas the TO structure varies in a nonmonotonic way which can be represented by three components: (*A*) at low pressures, (*B*) in the intermediate range, and (*C*) at high pressures. This behavior is somewhat similar to that observed in the isomorphic compounds GaP (Refs. 16 and 33), and in CuCl (Ref. 34), whose constituents are nearest neighbors of ZnS in the periodic table. Like in the cases of GaP and CuCl, it reflects a strong anharmonic coupling of the TO phonon with a background which corresponds to decay into the sum of two phonons [see Figs. 1(b) and 2].

B. Discussion

The deconvoluted FWHM of the LO and TO phonons at 16 K are shown vs pressure in Fig. 5. They can be treated, at this temperature, as arising from the standard second-order perturbation expression (Fermi's golden rule):[31]

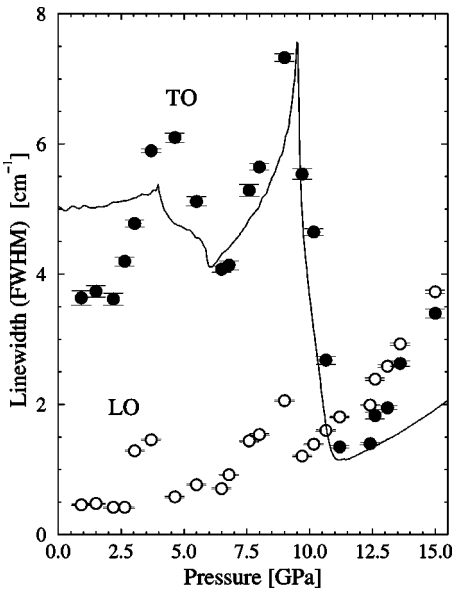

FIG. 5. Pressure dependence of the TO-phonon linewidth of $^{68}Zn^{32}S$ at 16 K and comparison to the corresponding portion of the INS-corrected two-phonon sum DOS extracted from Fig. 2(b).

$$\Gamma(\omega) = |V_3|^2 \rho_+^{(2)}(\omega)[1 + n(\omega_1) + n(\omega_2)], \qquad (3)$$

where $n(\omega_1)$ and $n(\omega_2)$ are the Bose-Einstein (BE) factors of the two frequencies of the summation mode into which ω decays with wave-vector conservation: $\omega = \omega_1 + \omega_2$ and $\rho_+^{(2)}(\omega)$ is the two-phonon sum DOS. For the TO phonons ω_1 and ω_2 correspond to TA and LA modes at or close to the edge of the BZ. We take here for the evaluation of the BE factors $\omega_{\mathrm{TA}} = 80\ cm^{-1}$ and $\omega_{\mathrm{LA}} = 195\ cm^{-1}$. With these frequencies, the BE factors are negligible at 16 K. However, at 80 K, $1 + n(\omega_1) + n(\omega_2) \simeq 1.34$, a fact which is reflected by the TO widths listed in Table III for 16 and 80 K.

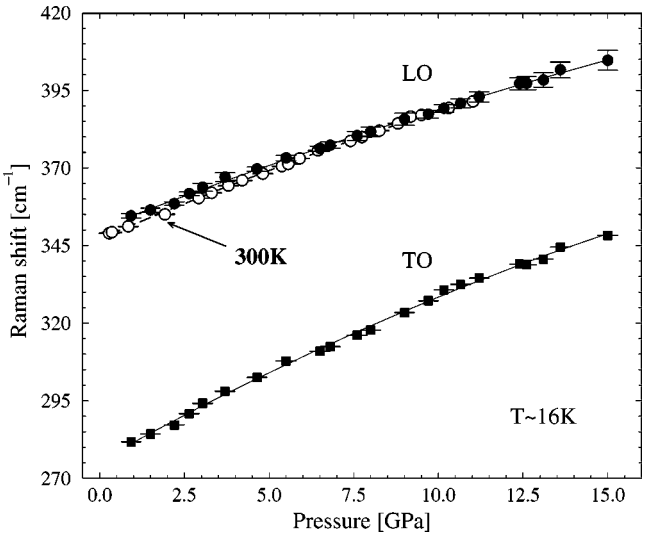

FIG. 6. Pressure dependence of the frequencies of the LO and TO phonons at 16 K and the LO phonon at 300 K (open circles). The frequencies of the TO mode at 300 K are not given here since they are strongly modified by anharmonic interaction (see Fig. 7).

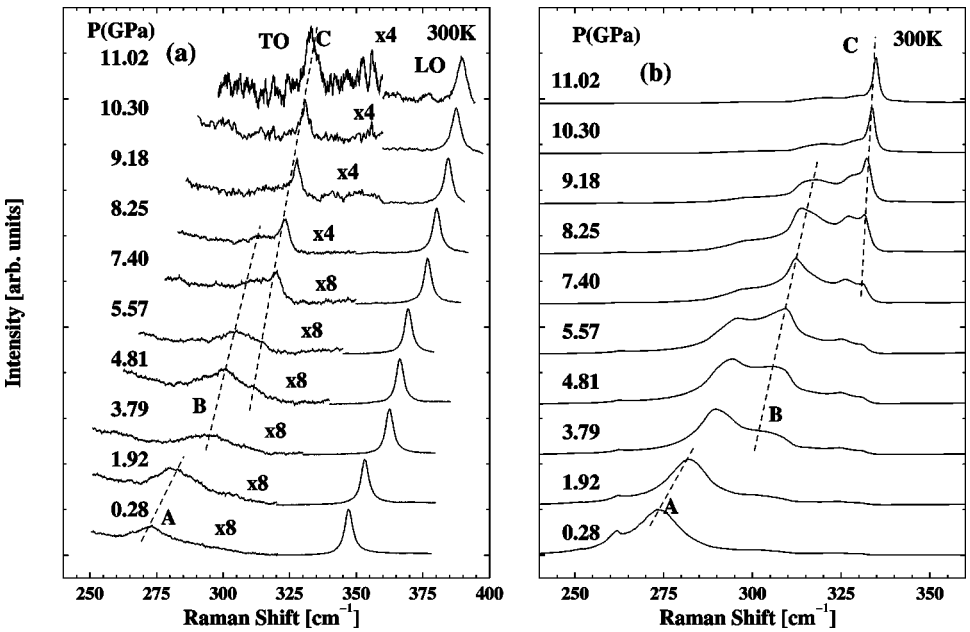

FIG. 7. (a) LO and TO Raman spectra of $^{68}Zn^{32}S$ measured at 300 K with the sample under several pressures. Note that the LO peak varies smoothly with pressure (its height has been normalized to one) while the TO peak varies in a nonmonotonic way which reflects the interaction with the two-phonon (sum) background. The three dashed lines approximately represent the variation with pressure of the different peaks contributing to the TO Fermi resonance. The resolution, not deconvoluted, is 1.7 cm^{-1} FWHM. (b) Simulation of the TO spectra of Fig. 7(a) as a Fermi resonance of the bare TO frequency with the corresponding two-phonon background.

We display in Fig. 5 a comparison of the two-phonon (sum) DOS $\rho_{+}^{(2)}[\omega_1(p)+\omega_2(p)=\omega_{TO}(p)]$ with the linewidth data for the TO phonons at 16 K. The DOS (solid curve) has been slightly modified so as to correct for discrepancies of about 20 cm^{-1} between the calculated dispersion relations and the INS data on which they are based.[14]

The two maxima and two minima observed in the FWHM correspond rather well to critical points in the DOS (maxima: $[TA_u+LA]_W$ and $[TA+LA]_X$; minima: $[TA+LA]_X$ and $[TA_u+LA]_K$ where the subscript "*u*" designates the upper of the two TA bands at either W or K). Using Eq. (3) and the two-phonon DOS normalized to six branches per primitive cell (i.e., the integral of the two-phonon DOS equal to 36), we obtain $|V_3|^2 \simeq 90$ cm^{-2}, rather close to the value found for GaP (57 cm^{-2}, Ref. 20) and CuCl (70 cm^{-2}, Ref. 21).

In trying to follow a similar procedure to analyze the pressure dependence of the LO-phonon widths shown in Fig. 5, we encountered some serious difficulties. The decay channels for these phonons involve $2LA_W$ overtones and $[TA+TO]_L$ combinations, whose frequency must also be readjusted to correct for the discrepancies with the INS data mentioned above. The adjustment, however, is different for each critical point: $2LA_W$ must be shifted up by 20 cm^{-1}, whereas $[TA+TO]_L$ must be shifted down by 5 cm^{-1}. As a result of these shifts, the frequencies of the two critical points reverse order and the shape of the DOS changes strongly. The two maxima shown for the LO widths in Fig. 5 correspond to the two critical points seen at 355 and 368 cm^{-1} in the corrected DOS of Fig. 2(b), whereas the increase in the FWHM at the highest pressures corresponds to the increase in DOS in Fig. 2(a) above 370 cm^{-1}. Using Eq. (3) we find for the LO-phonon linewidth at zero pressure the average anharmonic constant $|V_3|^2 = 15$ cm^{-2}.

At 300 K the BE factors for the TO modes amount to ≈ 3.8. This produces a strong enhancement of the anharmonic decay, i.e., a strong coupling of the LO phonon with the two-phonon continuum, so that the linewidth can no longer be represented at each pressure by a constant [given by Eq. (3) evaluated at $\omega=\omega_{TO}(p)$]. Like in the cases of CuCl and GaP we must insert in the Lorentzian expression for the line shape

$$A(\omega)=\frac{\Gamma_T(\omega)/2}{[\omega_0-\omega-\Delta_T(\omega)]^2+[\Gamma_T(\omega)/2]^2} \tag{4}$$

values of $\Gamma_T(\omega)/2$ (the imaginary part of the anharmonic phonon self-energy) and $\Delta_T(\omega)$ (its real part) which depend on frequency. Using for $\Gamma_T(\omega)=\Gamma(\omega)[1+n(\omega_1)+n(\omega_2)]$, $\Gamma(\omega)$ being obtained from the solid curve in Fig. 5 based on the INS-corrected two-phonon DOS between 280 and 338 cm^{-1}, and calculating $\Delta_T(\omega)$ as the Hilbert transform of $\Gamma_T(\omega)$, we have generated, for 300 K, the curves of Fig. 7(b). These curves mimic, at least qualitatively, the experimental curves of Fig. 7(a). At low pressures, a broad (FWHM ≈ 12 cm^{-1}) but well-defined peak labeled *A* is seen. It shifts in frequency with increasing pressure to merge with a much broader structure labeled *B*. The intensity of this structure decreases above 6 GPa while a sharper peak appears tending, such as in the cases of GaP and CuCl, to the unrenormalized TO frequency (FWHM ≈ 4 cm^{-1} at 9.2 GPa). The experimental data of Fig. 7(a) suggest a broadening of this peak above 9.2 GPa which is not obvious in the modeling of Fig. 7(b), probably due to the limitations of the model.

Using the expression

$$e_T^2=\frac{\mu\epsilon_\infty V(\omega_{\mathrm{LO}}^2-\omega_{\mathrm{TO}}^2)}{4\pi}, \tag{5}$$

it is possible to calculate the value of the transverse effective charge, $e_T=1.8$ at 1 atm, and its dependence on pressure. In Eq. (5) V is the volume per molecule of ZnS, μ the reduced mass of the primitive cell, and ϵ_∞ the long-wavelength dielectric constant. Using the values of ω_{LO} and ω_{TO} given in

Eq. (2) and $\epsilon_\infty = 5.7$ (Ref. 35), and taking the logarithmic derivative of Eq. (5) we find the Grüneisen parameter of the effective charge γ_T:

$$\gamma_T = -\frac{d\ln e_T}{d\ln V} = \gamma_{\mathrm{LO}} + \frac{(\gamma_{\mathrm{LO}} - \gamma_{\mathrm{TO}})\omega_{\mathrm{TO}}^2}{\omega_{\mathrm{LO}}^2 - \omega_{\mathrm{TO}}^2} - \frac{1}{2}\left(\frac{d\ln \epsilon_\infty}{d\ln V} + 1\right). \tag{6}$$

By replacing into Eq. (6) the values of the mode Grüneisen parameters γ_{LO} and γ_{TO} obtained from Eq. (2) and $d\ln \epsilon_\infty / d\ln V = 0.21$ (Ref. 35) we find $\gamma_T = -0.86$. The negative sign of γ_T means that the charge $|e_T|$, and thus the ionicity of β-ZnS, decreases with increasing pressure, a situation which applies to most zinc-blende-type semiconductors (only known exception: SiC, Ref. 36). This value agrees reasonably well with $\gamma_T = -0.7$ and -1.0 found in the literature.[38,37]

VI. DEPENDENCE OF LO_Γ AND TO_Γ FREQUENCIES AND LINEWIDTHS ON ISOTOPIC MASSES

A strong dependence of the linewidths of some Raman phonons on isotopic mass has been observed for GaP (TO_Γ), CuCl (TO_Γ), CuBr (LO_Γ), and ZnO (E_2^{upper}).[20–22,31] It is related to the fact that the frequency of these phonons falls in a region in which the two-phonon DOS varies steeply with frequency. This is not the case for the TO phonons of ZnS [see Fig. 2(b)] and, in principle, no striking dependence of the FWHM is expected. Table III shows a marginal variation of the TO_Γ widths with isotopic composition. We have not been able to explain these variations on the basis of Fig. 2(b). At 300 K this failure may be related to the complicated nature of the TO_Γ line shape [Fig. 7(a)] which renders meaningless a simple fit to a Lorentzian, with a frequency independent Γ. At low temperatures, however, one may expect the simple Lorentzian treatment to work, as was the case for the pressure dependence of Γ (Fig. 5). We have not been able, however, to account for the differences (between 1.9 and 3.7 cm^{-1} FWHM) found in Table III at 16 K. The differences do not vary much with temperature, hence it is not possible to attribute them to higher-order anharmonic processes. Another possibility, namely, lattice defects such as stacking faults, is hard to verify.

The LO_Γ frequency of the natural sample falls in a steeper region of the two-phonon DOS. This region corresponds, after the correction illustrated in Fig. 2(b), mainly to $[\mathrm{TO}+\mathrm{TA}]_{\mathrm{L}}$ pairs of phonons whose frequency shifts from $^{64}Zn^{34}S$ to $^{68}Zn^{32}S$ only slightly more than that of the LO_Γ phonon (see Table II), a fact which explains the failure to observe a dependence of the LO-phonon linewidth on isotopic mass.

One may consider the possibility of an effect of isotopic disorder (in the $^{\mathrm{nat}}Zn^{\mathrm{nat}}S$ and, even more so, in the $^{68}Zn^{32}S_{0.5}^{34}S_{0.5}$) on the linewidths. Such dependence is also not evident in the data of Table III. The reason is likely to be that the corresponding frequencies fall at a threshold of the one-phonon DOS where this DOS vanishes. This reason was invoked to explain the lack of isotope disorder effect for the LO_Γ phonons of ZnSe (Ref. 39) and the very small effect ($\sim 0.2\ \mathrm{cm}-1$) observed for Si,[40] Ge,[41] and α-Sn.[42] For the TO_Γ phonons of ZnSe, however, a strong mass disorder effect is observed, because the TO_Γ frequency does not fall at a threshold of the one-phonon DOS but in the middle of a DOS band.[39] The mass disorder should not only contribute to the linewidth Γ but also to the corresponding real part of the self-energy Δ. This effect does not vanish at a threshold but rather reaches a maximum[39–42] which is positive if the one-phonon DOS lies mostly below the frequency under consideration and negative in the opposite case. When scaling the frequencies of Table III according to the square root of the masses we find that they all agree with each other to within $\pm 0.1\ \mathrm{cm}^{-1}$, except for those of the $^{68}Zn^{32}S_{0.5}^{34}S_{0.5}$ sample which deviate by -0.3 ($+0.8$) cm^{-1} for the TO (LO) peaks from the predictions obtained by scaling. This difference corresponds to the self-energy Δ due to mass disorder. The values of Δ calculated for the TO and LO Raman phonons in the $^{68}Zn^{32}S_{0.5}^{34}S_{0.5}$ sample are -0.3 and $+0.5\ \mathrm{cm}^{-1}$, respectively. For these calculations[15] we have used the one-phonon DOS obtained from the dispersion relations of Ref. 14 and eigenvector components equal to one for the intermediate states and $|\mathbf{e}_\Gamma|^2 = 0.67$ for the phonons at the Γ point. The latter eigenvectors follow from the conditions of center-of-mass conservation.

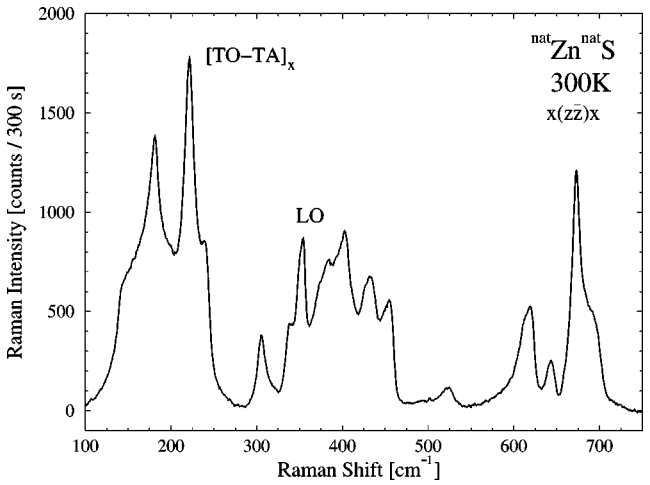

FIG. 8. Second-order Raman spectrum of natural ZnS at 300 K for the $x(\bar{z}\bar{z})x$ polarization [the notation $x(\bar{z}\bar{z})x$ is that of Ref. 44].

VII. SECOND-ORDER SPECTRA

The second-order spectrum of natural ZnS, measured at 300 K with the micro-Raman setup and a resolution of 2.5 cm^{-1}, is shown in Fig. 8. We chose for this spectrum the scattering configuration in which the incident and scattered polarizations are parallel to one of the crystal axes. In this configuration, both TO and LO phonons are Raman forbidden and do not overlap with neighboring two-phonon structure. The residual LO peak is probably due to the quadrupole-allowed intraband Fröhlich mechanism and remains weak because of being far away from resonance.

Figure 9 shows the unpolarized spectra of three isotopic samples plus the natural one within the (130–300)-cm^{-1} range (with the TO peak visible) and Fig. 10 shows the cor-

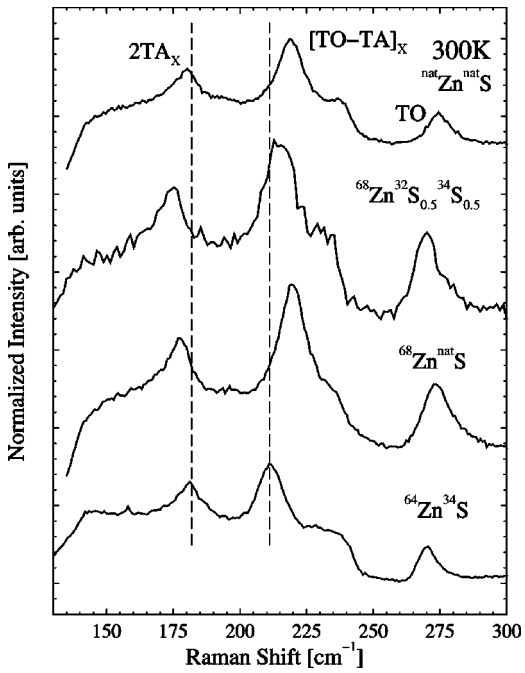

FIG. 9. Second-order Raman spectra at 300 K for several isotopic compositions in the range of the difference mode $[\mathrm{TO}-\mathrm{TA}]_X$. The dashed lines are guides to estimate the shifts of the critical points with the isotopic mass, as explained in the text.

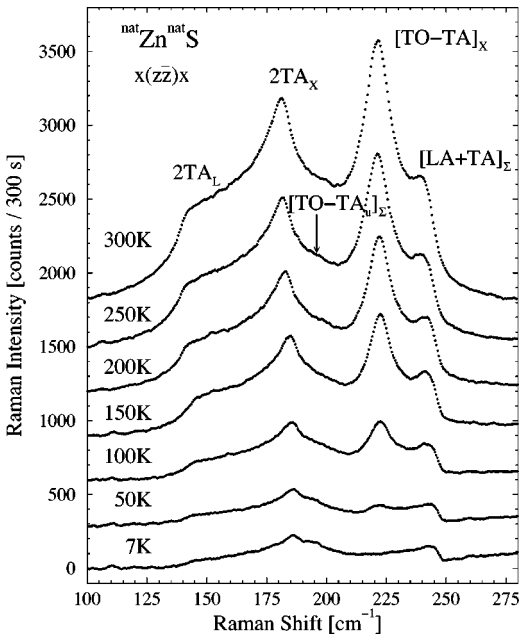

FIG. 11. Temperature dependence of second-order Raman spectra in the region of the $[\mathrm{TO}-\mathrm{TA}]_X$ critical point for natural ZnS. Note the strong increase in intensity of the difference mode as a function of temperature. The spectra have been arranged vertically with a spacing of 300 counts.

responding spectra in the (550–725)-cm^{-1} range. The large isotopic shifts of the peak at 219.5 cm^{-1} (natural sample), together with the pressure and temperature effects to be discussed below, allow us to conclusively assign this peak to differences of two phonons which, upon comparison with Table II, turn out to be TO-TA at the x point of the Brillouin zone. Note that the frequencies for the $[\mathrm{TO}-\mathrm{TA}]_X$ structure in the DOS's listed in Table II correspond rather well to those for the observed second-order peaks. Additional confirmation of the assignment of the $[\mathrm{TO}-\mathrm{TA}]_X$ 219.5-cm^{-1} scattering peak is obtained from Fig. 11 where the temperature dependence of the scattering in the $x(z\bar{z})\bar{x}$ configuration is displayed. Note that, contrary to the sum peaks ($2\mathrm{TA}_L$, $2\mathrm{TA}_X$, $[\mathrm{LA}+\mathrm{TA}]_\Sigma$), the peak at 219.5 cm^{-1} disappears at low temperatures as would be expected for scattering by the difference of two phonons, whose intensity follows the law

$$I(T)\propto n_2(1+n_1), \tag{7}$$

where n_1 and n_2 are the Bose-Einstein factors of the phonon being created and that being annihilated, respectively. The vanishing of I for $T\rightarrow 0$ follows from the vanishing of n_2: at $T=0$ no phonons can be annihilated. Our pressure measurements yield for the $[\mathrm{TO}-\mathrm{TA}]_X$ peak of the ^{68}Zn^{32}S sample the frequency

$$\omega([\mathrm{TO}-\mathrm{TA}]_X)=219.4(4)+6.1(6)p. \tag{8}$$

Although we shall not present here detailed curves showing the intensities of the various two-phonon peaks vs T, we have also checked that the sum peaks follow the expected dependence:

$$I(T)\propto(1+n_1)(1+n_2). \tag{9}$$

The rather large pressure coefficient of Eq. (8) corresponds to the difference between the positive coefficient of TO_X and the negative one of TA_X, as already pointed out by Weinstein.[16]

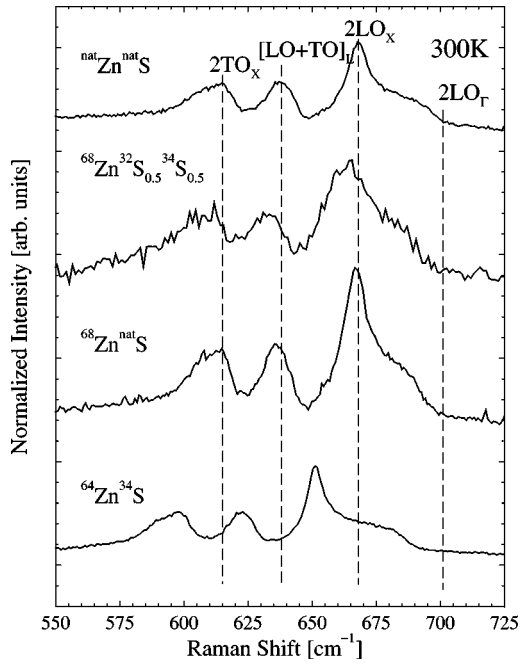

FIG. 10. Second-order Raman spectra at 300 K for several isotopic compositions corresponding to combinations of two optical modes. The dashed lines are guides to estimate the shifts of the critical points with the isotopic mass, as explained in the text.

TABLE IV. Measured frequencies of the second-order Raman peaks for the investigated isotopic compositions, in cm^{-1}.

Assignment	$^{64}Z^{34}S$	$^{nat}Zn^{nat}S$	$^{68}Zn^{nat}S$	$^{68}Zn^{32}S^{34}_{0.5}S_{0.5}$
$2LO_\Gamma$	692.4	700.0	699.2	695.5
$2LO_L$	681.0	692.7	689.2	685.6
$2LO_X$	651.1	667.9	667.0	664.2
$[LO+TO]_L$	622.4	637.7	636.1	632.5
$2TO_X$	597.8	614.6	614.0	607.3
$2TO_W$	590.6	607.3	607.6	
$[LO+LA]_\Sigma$	510.3	517.0	512.3	512.1
$[TO_l+LA]_\Sigma$	484.9	482.7	484.0	
$[LO+TA]_L$	443.6	449.7	446.8	447.0
$[LO+TA]_X$	412.0	419.8	418.0	417.0
$[TO+TA]_X$	391	397	396	393
$2LA_\Sigma$		380 [a]		
Not assigned		346 [a]		
Not assigned		336 [a]		
$[LA+TA_u]_{W,\Sigma}$	312	312 [a]		
$[LA+TA_l]_W$		304	300	
$2TA_\Sigma$	238.4	239	235.9	234.8
$[TO-TA_u]_\Sigma$		198 [a]		
$[TO-TA]_X$	211.4	218.9	219.5	215.0
$2TA_X$	181.3	180.0	177.3	175
$2TA_L$	142.2	141.7	140.8	140

[a]Data obtained from measurements on natural ZnS by using several scattering geometries.

We have tentatively assigned the small structure which appears in Fig. 11 at 198 cm^{-1} to another difference mode, namely, $[TO-TA_u]_\Sigma$, i.e., to the second strongest peak in Fig. 1(a). It disappears at low temperature, but it remains too weak at 300 K to make sure that its intensity follows Eq. (7). We did not investigate this scattering configuration for the isotopic samples; hence the assignment must remain tentative. Note the excellent agreement between the measured frequencies of the $2TA_L$ (141.7 cm^{-1}), $2TA_X$ (180.0 cm^{-1}), and the calculated ones (143 cm^{-1}, after adding 6 cm^{-1} for the dispersion relations correction, and 180 cm^{-1}, respectively). The measured and calculated isotope shifts also agree with each other. Agreement is also found for the $[2TA_u]_\Sigma$ modes, especially after applying the correction to the frequencies of Table II.

The peak labeled $2LA_W$ in Table IV (at 380 cm^{-1} for the $^{64}Zn^{34}S$ sample) corresponds to the 359-cm^{-1} $2LA_W$ peak of Table II after adding the correction of the dispersion relations, which in this case amounts to 24 cm^{-1}. Similar agreement is found for the $[TO+TA]_X$ frequencies of Tables II and IV and their isotopic shift; in this case no correction is needed. Note that the sign reversal of the shifts occurs between 316 cm^{-1} and 397 cm^{-1}, in agreement with Table II and the discussion of Sec. III.

We could go on comparing the measured frequencies (Table IV) with the calculated ones (Table II plus corrections) but this can be easily done by the reader. Instead, we discuss the frequencies of some of the features for which the corrections of the calculation are absolutely necessary for the assignment. We have already mentioned, in connection with Table III, that such corrections are needed for the TO_Γ and LO_Γ phonons. For the corresponding two-phonon states we measure (natural sample) $2LO_\Gamma = 700$ cm^{-1}, which agrees perfectly with the corrected calculation ($712-12 = 700$ cm^{-1}). The isotope shifts of this peak are also interesting: contrary to most other peaks the natural sample has the highest frequency, due to the fact that it shifts like the reduced mass. The $2LO_X$ peak is measured at 668 cm^{-1} for the natural sample whereas the calculated frequency is $697-24=673$ cm^{-1} (the remaining discrepancy is to be attributed to uncertainties in the correction). The $[LO+TO]_L$ peak, measured at 638 cm^{-1}, is calculated to be at $647-6 = 641$ cm^{-1}. We leave any further comparison of the results of Table II (plus corrections) and Table IV to the reader.

VIII. CONCLUSIONS

We have presented a comprehensive study of the one- and two-phonon Raman spectra of β-ZnS and their dependence on pressure, temperature, isotopic mass disorder, and, to a limited extent, laser frequency. The dependence on laser frequency enables us to attribute the vanishing of the first-order TO peak at 1.95 eV to a cancellation between a nonresonant global background and the resonant effect of the E_0 edge. This realization allows us to correct the $d_0=4$ eV first-order electron-phonon deformation potential to a value of about 18 eV, closer to the calculated values ($d_0 \simeq 24$ eV). Measurements of the frequencies and linewidths of the TO and LO Raman peaks reveal that they shift like the reduced mass of the primitive cell, except for small self-energy corrections due to the sulfur mass disorder in the $^{68}Zn^{32}S^{34}_{0.5}S_{0.5}$ sample. The latter effects are also not conclusively observed in the corresponding linewidths, a fact that can be accounted for on the basis of the two-phonon densities of states.

The dependence of the TO and LO peaks on pressure, measured at 16 K as well as at 300 K, reveals a number of interesting features which can be attributed to anharmonic decay into two phonons. The pressure effects are particularly strong for the TO phonons at room temperature: the measurements, and also calculations based on the two-phonon density of states, reveal that the TO phonon is strongly coupled to the two-phonon background (consisting mostly of TA+LA combinations), such as a Fermi resonance which changes gradually upon application of pressure. At pressures higher than 10 GPa the TO frequency moves out of the two-phonon region and sharpens up, thus recovering its decoupled intensity.

The measurements vs temperature, pressure, and isotopic mass help us to attribute the peaks in the second-order Raman spectra to calculated structures in the two-phonon density of states. A strong difference mode $[TO-TA]_X$ is found at 219 cm^{-1} for the natural sample and a much weaker one, assigned to $[TO-TA_u]_\Sigma$ scattering, at 199 cm^{-1}. All other observed modes are found to correspond to sum modes (overtones and combinations). They are assigned to peaks in the calculated two-phonon DOS.

ACKNOWLEDGMENTS

We thank C. Trallero-Giner for a critical reading of the manuscript. Thanks are also due to H. Vogt for performing Raman measurements during the initial phase of this work. One of the authors (A.C.) thanks B. Keimer for the loan of a spectrometer at a time of great distress. T.M.R. acknowledges a UNC Pembroke research travel grant. Work at U. Buffalo was partially supported by the UB CAPEM center.

[1] C. Frondel, and C. Palache, Science **107**, 602 (1947).
[2] M. Farkas-Jahnke, Acta Crystallogr. **18**, 571 (1965).
[3] O. Brafman, and I.T. Steinberger, Phys. Rev. **143**, 501 (1966).
[4] R. Lauck (unpublished).
[5] T. Deutsch, in *Proceedings of Sixth International Conference on Phys. Semic., Exeter* (Institute of Physics and Physical Society, London, 1962), p. 505.
[6] L. Couture-Mathieu and J.P. Mathieu, Compt. Rend. **236**, 371 (1953).
[7] O. Brafman and S.S. Mitra, Phys. Rev. **171**, 931 (1968).
[8] W.G. Nilsen, Phys. Rev. **182**, 838 (1969).
[9] R. E. Tallman, T. M. Ritter, B. A. Weinstein, A. Cantarero, J. Serrano, R. Lauck, and M. Cardona, Phys. Status Solidi B (to be published).
[10] H. Poulet, W. E. Klee, J. P. Mathieu, in *Proceedings of the International Conference on Lattice Dynamics, Copenhagen* (Pergamon Press, New York, 1965), p. 337.
[11] C.A. Arguello, D.L. Rousseau, and S.P.S. Porto, Phys. Rev. **181**, 1351 (1969).
[12] L.A. Feldkamp, D.K. Steinman, N. Vagelatos, J.S. King, and G. Venkataraman, J. Phys. Chem. Solids **32**, 1573 (1971).
[13] N. Vagelatos, D. Wehe, and J.S. King, J. Chem. Phys. **60**, 3613 (1974).
[14] B.D. Rajput and D.A. Browne, Phys. Rev. B **53**, 9052 (1996).
[15] F. Widulle, J. Serrano, and M. Cardona, Phys. Rev. B **65**, 075206 (2002).
[16] B.A. Weinstein, Solid State Commun. **24**, 595 (1977).
[17] B. A. Weinstein, in *High Pressure Science and Technology*, edited by K.D. Timmerhaus and M. S. Barber (Plenum Press, New York, 1979), Vol. 1, p. 141.
[18] R.L. Schmidt, K. Kunc, M. Cardona, and H. Bilz, Phys. Rev. B **20**, 3345 (1979).
[19] J.M. Calleja, H. Vogt, and M. Cardona, Philos. Mag. A **45**, 239 (1982).
[20] F. Widulle, T. Ruf, A. Göbel, E. Schonherr, and M. Cardona, Phys. Rev. Lett. **82**, 5281 (1999).
[21] A. Göbel, T. Ruf, C.T. Lin, M. Cardona, J.C. Merle, and M. Joucla, Phys. Rev. B **56**, 210 (1997).
[22] J. Serrano, T. Ruf, F. Widulle, C.T. Lin, and M. Cardona, Phys. Rev. B **64**, 045201 (2001).
[23] W. Pałosz, M.J. Kozielski, and B. Pałosz, J. Cryst. Growth **58**, 185 (1982).
[24] R. Nitsche, H.U. Bölsterli, and M. Lichtensteiger, J. Phys. Chem. Solids **21**, 199 (1961).
[25] H. Hartmann, J. Cryst. Growth **42**, 144 (1977).
[26] W. Pałosz, J. Cryst. Growth **60**, 57 (1982).
[27] R. Zuo and W.K. Wang, J. Cryst. Growth **236**, 687 (2002); **236**, 695 (2002).
[28] H.K. Mao, J. Xu, and P.M. Bell, J. Geophys. Res., [Solid Earth Planets] **91**, 4673 (1986).
[29] B.A. Weinstein, Philos. Mag. B **50**, 709 (1984).
[30] In order to help the assignment and make it more reliable we have performed the analysis by plotting separately the individual branches of the dispersion relations.
[31] J. Serrano, F. Widulle, A.H. Romero, M. Cardona, R. Lauck, and A. Rubio, Phys. Status Solidi B **260**, 235 (2003); J. Serrano, F.J. Manjón, A.H. Romero, F. Widulle, R. Lauck, and M. Cardona, Phys. Rev. Lett. **90**, 055510 (2003).
[32] A. Blacha, H. Presting, and M. Cardona, Phys. Status Solidi B **126**, 11 (1984).
[33] S. Ves, I. Loa, K. Syassen, F. Widulle, and M. Cardona, Phys. Status Solidi B **223**, 241 (2001).
[34] C. Ulrich, A. Göbel, K. Syassen, and M. Cardona, Phys. Rev. Lett. **82**, 351 (1999).
[35] *Landolt-Börnstein Tables*, edited by O. Madelung, M. Schulz, and H. Weisseds (Springer, Berlin, 1982), Vol. 17b.
[36] E. Anastassakis and M. Cardona, in *High Pressure in Semiconductor Physics II*, edited by W. Paul and T. Suski (Academic Press, New York, 1998), Vol. 58.
[37] B. A. Weinstein and R. Zallen, in *Light Scattering in Solids*, edited by M. Cardona and G. Guntherodt (Springer, Berlin, 1984), Vol. IV, p. 463.
[38] M. Cardona, J. Phys. (Paris) **45**, 29 (1984).
[39] A. Göbel, T. Ruf, J.M. Zhang, R. Lauck, and M. Cardona, Phys. Rev. B **59**, 2749 (1999).
[40] F. Widulle, T. Ruf, M. Konuma, I. Silier, M. Cardona, W. Kriegseis, and V.I. Ozhogin, Solid State Commun. **118**, 1 (2001).
[41] J.M. Zhang, M. Giehler, A. Göbel, T. Ruf, M. Cardona, E.E. Haller, and K. Itoh, Phys. Rev. B **57**, 1348 (1998).
[42] D.T. Wang, A. Göbel, J. Zegenhagen, and M. Cardona, Phys. Rev. B **56**, 13 167 (1997).
[43] See http://www.webelements.com/
[44] D.L. Rousseau, R.P. Bauman, and S.P.S. Porto, J. Raman Spectrosc. **10**, 253 (1981).